

Resolving the Periods of the Asynchronous Polar 1RXS J083842.1–282723

J. P. HALPERN¹

¹*Department of Astronomy and Columbia Astrophysics Laboratory, Columbia University, 550 West 120th Street, New York, NY 10027-6601, USA; jph1@columbia.edu*

ABSTRACT

1RXS J083842.1–282723 is a nearly synchronous magnetic cataclysmic variable with a simple X-ray light curve. While its orbital period was fairly well established at $P_{\text{orb}} = 98.4$ minutes from optical spectroscopy, indirect estimates of $P_{\text{spin}}/P_{\text{orb}}$ ranged from 0.90 to 0.96 because the short X-ray light curves could not determine the beat period to a factor of 2. We analyze a recent 50 day TESS observation, and ground-based optical time-series photometry spanning 9 years, that together measure precise beat, orbit, and spin periods and enable the X-ray and optical modulations to be phase aligned. Although the X-ray light curves do not distinguish between a beat period of 16.11 or 32.22 hours, all of the optical evidence favors the longer value, with complete pole switching of accretion every half beat cycle. This would require $P_{\text{spin}}/P_{\text{orb}} = 0.952$. Long-term optical monitoring also shows a decline in accretion rate, and a change in the beat-folded light curve. It would be useful to obtain a new X-ray/optical observation of at least 32 hours duration to examine any associated change in accretion structure, and confirm the spin and beat periods.

1. INTRODUCTION

Cataclysmic variables (CVs) are accreting binaries in which a dwarf star donates mass to a white dwarf (WD) via Roche-lobe overflow. A strong WD magnetic field can truncate an accretion disk at the magnetospheric boundary, or even prevent a disk from forming. In polars (AM Her stars), the magnetic field is strong enough to channel an accretion stream directly from the donor onto a magnetic pole, and lock the WD rotation to the binary orbit ($P_{\text{spin}} = P_{\text{orb}}$). Intermediate polars (IPs) have weaker B -fields; the WD poles(s) can be fed either from a truncated disk, a diskless stream, or a combination of both (disk-overflow stream). The spin of the WD in an IP is detected as a coherent oscillation in X-ray or optical emission at a period shorter than the orbital period of the binary, typically with $P_{\text{spin}} \leq 0.1 P_{\text{orb}}$.

A group of four “asynchronous polars” (APs), have spin and orbital periods that differ by $< 2\%$. One of these, V1500 Cyg, had a nova explosion in 1975, and because it is generally observed that APs are evolving toward synchronism on times scales of 100–13,000 yr (Myers et al. 2017; Littlefield et al. 2023a) it is plausible that nova eruptions perturbed the spin of the WD. A fifth member of this class is SDSS J085414.0+390537 (Kolbin et al. 2024).

Several magnetic CVs have been discovered with greater degree of asynchronism than the APs. IGR J19552+0044 (Tovmassian et al. 2017), SDSS J084617.1+245344, SDSS J134441.8+204408

(Littlefield et al. 2023a,b), and “Paloma” (Schwarz et al. 2007; Joshi et al. 2016; Littlefield et al. 2023a) have $P_{\text{spin}} = (0.87 - 0.97) P_{\text{orb}}$. It is unlikely that nova eruptions could perturb the spin by this much. But it is not clear whether these objects are pre-polars approaching synchronism, or stream-fed IPs whose spins are in stable equilibrium.

Fundamental to the life cycle of an mCV is the change of its equilibrium spin period as it evolves to shorter orbital period. In numerical simulations of accretion and spin equilibrium, Norton et al. (2004, 2008) concluded that $P_{\text{spin}}/P_{\text{orb}}$ should increase as P_{orb} decreases, and proceed to synchronism once $P_{\text{spin}}/P_{\text{orb}} > 0.6$. That most of the nearly synchronous mCVs have short orbital periods where IPs are rare, below the 2–3 hour period gap, supports the theory. Such compact systems are thought to accrete from a thin ring near the edge of the Roche lobe of the white dwarf. However, the values of the parameters of the theory, particularly the stellar mass ratio of 0.5, were chosen when nearly all IPs were known to have $P_{\text{spin}}/P_{\text{orb}} < 0.6$ (with the exception of EX Hya at 0.68). This choice had the effect of “predicting” that IPs with $0.6 < P_{\text{spin}}/P_{\text{orb}} < 1$ should be rare. But the number of recent asynchronous discoveries suggests that they are not so rare, and that spin equilibrium is possible at most if not all values of $P_{\text{spin}}/P_{\text{orb}}$. This could occur if the mass ratio is < 0.5 , as it would be at small orbital periods, and also if the magnetic moment

of the secondary is weak, preventing the system from synchronizing (Norton et al. 2004).

Two more members of this family, Swift J0503.7–2819 (Halpern 2022; Rawat et al. 2022; Pradeep et al. 2024) and 1RXS J083842.1–282723 (Rea et al. 2017; Halpern et al. 2017, hereafter Paper 1) have uncertain degrees of asynchronism because X-ray coverage of their spin-orbit beat periods was not complete. The favored interpretation of X-ray and optical data on Swift J0503.7–2819 yields $P_{\text{spin}} = 0.803 P_{\text{orb}}$. The subject of this paper is a proposed solution for 1RXS J083842.1–282723 (hereafter RX J0838.7–2827) enabled by TESS, the the Transiting Exoplanet Survey Satellite (Ricker et al. 2015).

The position of RX J0838.7–2827 is (Gaia-CRF3, epoch 2016.0) R.A.=08^h38^m43^s.3315, decl.=−28°27′00″.944 (Gaia Collaboration et al. 2016, 2023). Its parallax is 6.3855 ± 0.0828 mas, corresponding to a distance of 157 pc. Proper motion components are $(\mu_{\alpha} \cos \delta, \mu_{\delta}) = (-16.93 \pm 0.07, +12.46 \pm 0.08)$ mas yr^{−1}. Its average X-ray luminosity is $\approx 2 \times 10^{31}$ erg s^{−1} in the 0.3–10 keV band from XMM-Newton (Paper 1).

Section 2 reviews the X-ray light curves of RX J0838.7–2827 and their original interpretations, followed by analysis of the recent TESS observation and long-term ground-based optical timing of RX J0838.7–2827 that refine the periods to high precision. Section 3 further evaluates the alternative identifications of the beat and spin periods. Conclusions and suggestions for further study of this variable object are presented in Section 4.

2. PERIODS FROM X-RAY AND OPTICAL

2.1. X-ray Light Curves (2015, 2016)

RX J0838.7–2827 was observed twice by XMM-Newton and once by Chandra (Paper 1); we review the resulting interpretations here. The longest of the XMM-Newton light curves is reproduced in Figure 1. The peaks and dips in the X-ray light curve suggest self-occultation by the rotating white dwarf of a stream-fed emitting spot whose accretion rate is strongly modulated at the longer beat frequency between spin and orbit. But the observation was not long enough to resolve well the spin and orbit. Rea et al. (2017) interpreted the blended pair of peaks around 15 cycles day^{−1} in the X-ray periodogram of Figure 1 as nearly synchronous spin (ω) and orbital (Ω) frequencies, and a peak near 1.6 cycles day^{−1} as the beat frequency, $\Omega_{\text{beat}} = \omega - \Omega$, corresponding to a beat period of ≈ 15 hours. The beat-modulated intensity could be caused switching of the accretion to an unseen “lower” pole, and back to the upper pole within one beat cycle. We denote this scenario “Case A.”

Noting that the spin period in Case A does not match well the actual spacing between the X-ray pulses, Paper 1 outlined a “Case B,” in which the time between adjacent dips suggests a slightly longer spin period that falls midway between the blended pair in the periodogram. Assuming that both poles are visible, and switching of accretion between them happens during a minimum of the beat modulation, the beat period is twice as long as in Case A. The second half of the beat cycle, which was not completely covered, is emission from the second pole. In the event of such complete pole switching, the spin signal ω is suppressed in the power spectrum, being replaced by the two sidebands $\omega \pm \Omega_{\text{beat}} = \Omega$ and $2\omega - \Omega$ (Wynn & King 1992). These two are the Case B identifications of the split peak.

In Paper 1 the peak in the periodogram at ≈ 1.6 cycles day^{−1} was interpreted as $3(\omega_{\text{B}} - \Omega)$. This, however, was based on imprecise knowledge of the spin or beat periods. The subsequent optical observations discussed below show that this peak is contributed primarily by $2(\omega_{\text{B}} - \Omega)$. Note that the values of the frequencies marked in Figure 1 are taken from the precise optical results listed in Tables 1 and 2. A spot model created by Wang et al. (2020) using the results of Paper 1 to match the X-ray light curve and power spectrum could be revised using these new values.

The difference between Case A and Case B is indicated by the tick marks above the X-ray light curve. The orbital period is the same in both cases, and agrees with optical radial velocity spectroscopy (Paper 1). The alternative spin periods are illustrated by the red (Case A) and blue (Case B) tick marks, with Case B corresponding to complete pole switching between each half of the beat cycle. This is exactly the dilemma of whether to identify the peak to the right of Ω in the periodogram as ω_{A} or $2\omega_{\text{B}} - \Omega$.

2.2. TESS (2023 January 18 – March 10)

A 50 day light curve of RX J0838.7–2827 at 2 minute cadence was obtained by the Transiting Exoplanet Survey Satellite (TESS; Ricker et al. 2015) in its sectors 61 and 62, starting on 2023 January 18. The average magnitude derived from the PDCSAP (Pre-search Data Conditioning Simple Aperture Photometry) fluxes is 18.2, consistent with simultaneous ground-based *r*-band observations presented in Section 2.3. We merged the two sectors’ light curves to calculate the periodogram in Figure 1. It has prominent narrow peaks, listed in Table 1 corresponding to the ones detected but not clearly resolved by the short XMM-Newton observation. The strongest signal, at 14.63 cycles day^{−1}, is consistent with the orbital frequency Ω first determined from optical

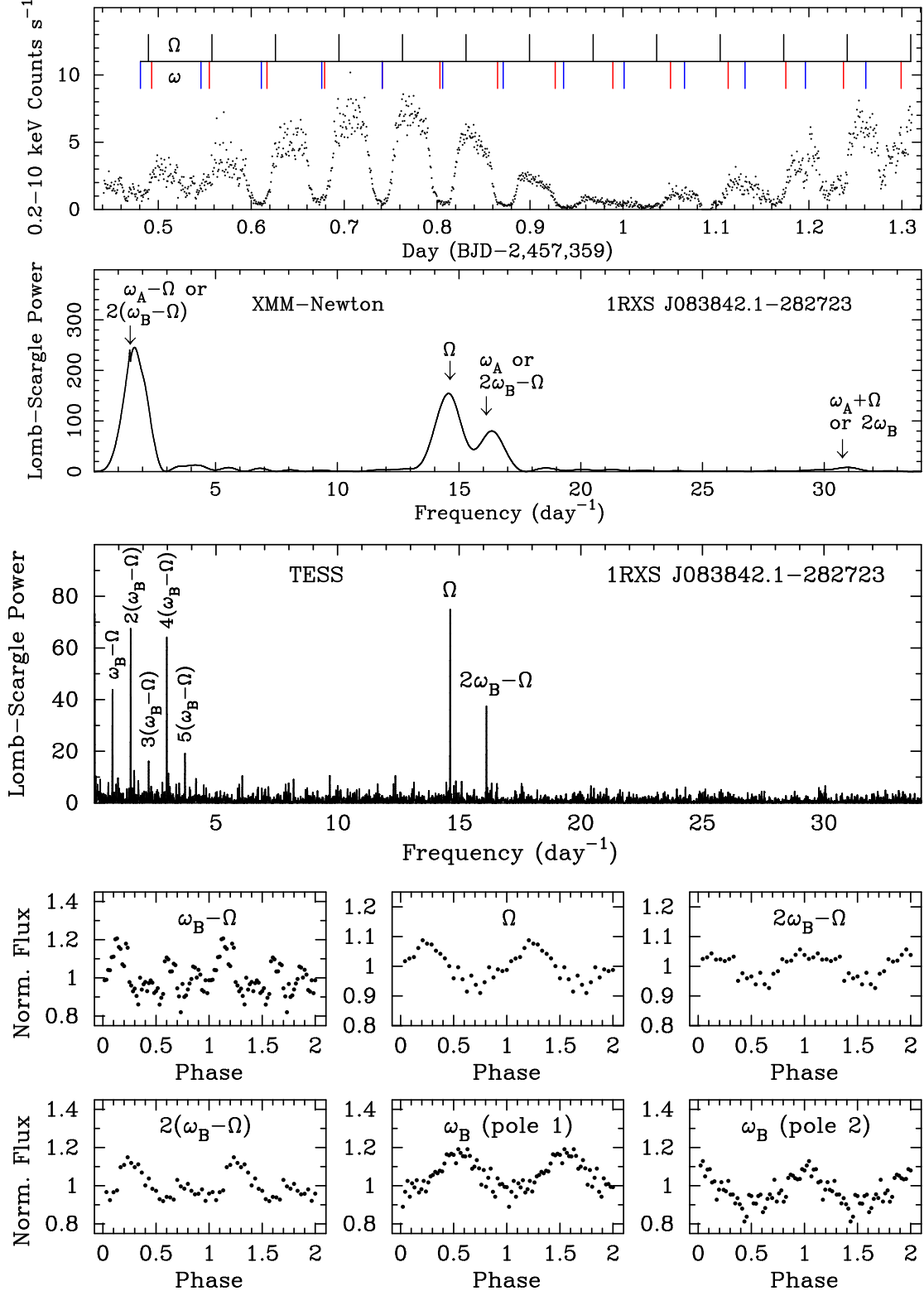


Figure 1. Top: From the XMM-Newton observation of RX J0838.7–2827 on 2015 December 2, a combined EPIC pn and MOS 0.2–10 keV light curve in 60 s bins. There is a short gap in the data at day 1.09. The alternative spin cycles are marked in red (Case A: short beat cycle) and blue (Case B: long beat cycle), where blue corresponds to pole switching at each minimum of the beat cycle. Middle: Periodograms of the XMM-Newton light curve and 50 day TESS observation. Peaks in XMM-Newton are identified in either Case A (upper label) or Case B (lower label), while TESS favors Case B. Bottom: TESS light curve folded on the Case B beat, orbital, and spin periods, revealing different fluxes from accreting poles 1 and 2.

radial velocity spectroscopy, while a peak at 16.12 cycles day^{-1} is either the spin ω_A or $2\omega_B - \Omega$.

There are five equally spaced peaks between 0.745 cycles day^{-1} and 3.726 cycles day^{-1} that can be attributed to the beat frequency $\omega_B - \Omega$ and its harmonics. These may help to resolve the ambiguous identity of the 16.12 cycles day^{-1} peak. If 0.745 cycles day^{-1} is $\omega_B - \Omega$, then the peak at 16.12 cycles day^{-1} should be $2\omega_B - \Omega$. Otherwise, if 16.12 cycles day^{-1} were ω_A , then 0.745 cycles day^{-1} would have to be $\frac{1}{2}(\omega_A - \Omega)$. This and the higher half-integer harmonics would not have a natural interpretation. Thus, the TESS peaks in Figure 1 are labeled according to their Case B identifications, in which there are two minima per beat cycle and complete pole-switching occurs during each minimum.

The bottom panels in Figure 1 show the TESS data folded on the major periods in the power spectrum. The epochs of phase zero are defined in Section 2.5 and Table 3. When deciding between Case A and Case B, evidence of non-identical poles would support Case B’s complete pole switching. Even if the spin frequency is not present in the total power spectrum, pulses from opposite poles can be detected by folding half or less of the Case B beat cycle — in this application we choose 40% — on the inferred spin period, and sliding the folding window through the beat cycle in search of maximum power in the spin modulation.

Using this method we found two regions, approximately 180° apart in longitude, with pulsed fractions of $\approx 10\%$ but differing by $\approx 10\%$ in average flux. This small but significant difference is what contributes power to and identifies 0.745 cycles day^{-1} as the fundamental beat frequency $\omega_B - \Omega$. This, in turn, requires the 16.12 cycles day^{-1} peak to be $2\omega_B - \Omega$ rather than ω_A . Thus, TESS provides independent evidence in favor of Case B. Note that the beat cycle of frequency $\omega_B - \Omega$ is complex in TESS, comprising four peaks, unlike the simpler beat structure in X-rays. This explains why even multiples of the beat frequency are strong in TESS, and suggests that the accretion structure changed between 2015 and 2023.

2.3. Ground-based Optical (2014–2023)

Paper 1 reported a spectroscopic period of 0.068342(3) day from strong, single-peaked Balmer and He I emission lines, which we identified as the orbital period. The radial velocity amplitude was $274 \pm 16 \text{ km s}^{-1}$. Time-series photometry collected for 2–7 hours per night on six nights in 2014–2016 in various filters showed oscillations with a period of ≈ 0.07 day and changes of ≈ 1.5 mag between adjacent nights, corresponding to

Table 1. TESS Observed and Inferred Frequencies

Frequency (day^{-1})	Period	Case A	Case B
Observed			
0.7452(22)	32.206(95) hr	$\frac{1}{2}(\omega_A - \Omega)$	$\omega_B - \Omega$
1.4918(15)	16.088(16) hr	$\omega_A - \Omega$	$2(\omega_B - \Omega)$
2.2317(35)	10.754(17) hr	$\frac{3}{2}(\omega_A - \Omega)$	$3(\omega_B - \Omega)$
2.9782(17)	8.0586(46) hr	$2(\omega_A - \Omega)$	$4(\omega_B - \Omega)$
3.7262(29)	6.4409(50) hr	$\frac{5}{2}(\omega_A - \Omega)$	$5(\omega_B - \Omega)$
14.6290(15)	98.435(10) min	Ω	Ω
16.1202(23)	89.329(13) min	ω_A	$2\omega_B - \Omega$
Inferred			
15.3746(27)	93.661(16) min	...	ω_B

modulation at the X-ray beat cycle. Subsequent to that study, we obtained time series photometry on 21 nights between 2016 December and 2023 January using either the 2.4 m or 1.3 m telescope of the MDM Observatory, and on two nights using a CTIO 1 m telescope of the Las Cumbres Observatory global telescope network (LCOGT), all in an SDSS r filter with 5 min cadence.

Coherent power-spectrum analysis (Figure 2) of the combined 29 light curves spanning 9 years shows periods corresponding to the strongest peaks in the TESS periodogram, but with much higher precision, as listed in Table 2. Although 1-year aliases are also consistent with the TESS periods at $2(\omega_B - \Omega)$, Ω , and $2\omega_B - \Omega$, only the highest peak in each case gives consistent phasing of all of the optical and X-ray data. This can be seen by comparing the folded light curves in the insets of Figure 2 with the folded TESS light curves in Figure 1. Note that only $2(\omega_B - \Omega)$ is detected in the ground-based periodogram because it has higher power, but we fold on $\omega_B - \Omega$ in Figure 2.

The only major difference between the folds of the TESS and ground-based data is the modulation at the beat period $\omega_B - \Omega$. While the TESS fold in Figure 1 shows four peaks, the ground-based fold has two unequal peaks of higher amplitude. TESS observed during a historical minimum state (see Section 2.4), while the ground-based observations are concentrated in earlier years when the star was brighter. The beat amplitude and profile may be sensitive to the average accretion rate in a way that reduces the amplitude and increases the complexity of the accretion flow when the accretion rate is lower.

The 29 individual optical light curves are shown in Figure 3, folded on the Case B spin period, which allows

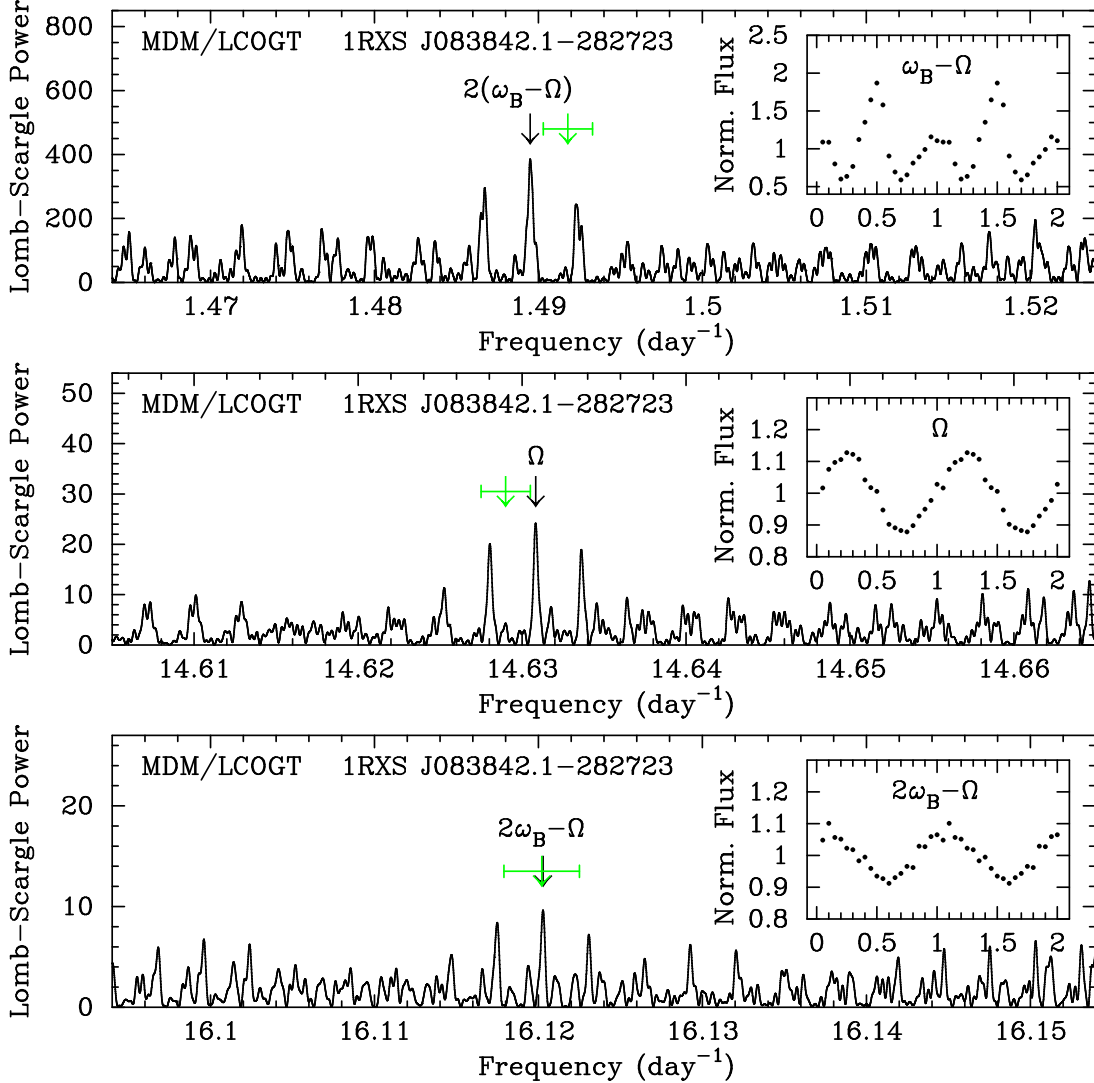


Figure 2. Periodograms of MDM and LCOGT data spanning 2014–2023, showing probable detections of the main periods also found by TESS and assigned their Case B identifications. Green symbols mark the values and uncertainties from TESS. One-year aliases flank the highest peaks. Inserts are the light curves folded at the highest MDM peak, except that the beat frequency ($\omega_B - \Omega$) is half the frequency of the detected peak in the upper panel.

the simplest phase relationship. The spin pulses come from either pole 1 or pole 2, corresponding to peaks at integer or half-integer rotations, respectively. In contrast, folding on the Case A spin period (not shown) does not produce consistent phasing. Peaks fall as far as 0.25 cycles from their expected location, similar to the X-ray light curve when interpreted in Case A.

On several nights when the star was faint, pulses were very weak, which we attribute to a minimum of the accretion rate in the beat cycle. On two nights it is possible to see pole switching taking place at a beat minimum, where peaks come 0.5 cycles apart (2016 March 17) or 1.5 cycles apart (2017 December 16). The four most recent light curves, in 2023 January, are simultaneous with the TESS observation, which directly confirms

their phasing, and the fact that the beat amplitude is smaller than in 2014–2019. The lack of data in the years 2020–2022 obscures any details of the transition.

2.4. ATLAS (2015–2023)

We downloaded photometry of RX J0838.7–2827 from the Asteroid Terrestrial-impact Last Alert System (ATLAS; Tonry et al. 2018) forced photometry server, which is useful for documenting the long-term optical behavior of RX J0838.7–2827. After filtering out points with uncertainties > 0.3 mag, there are 1412 observations in the “orange” *o* filter (560–820 nm) and 543 observations in the “cyan” *c* (420–650 m) filter between 2015 October 26 and 2024 January 1. These data are

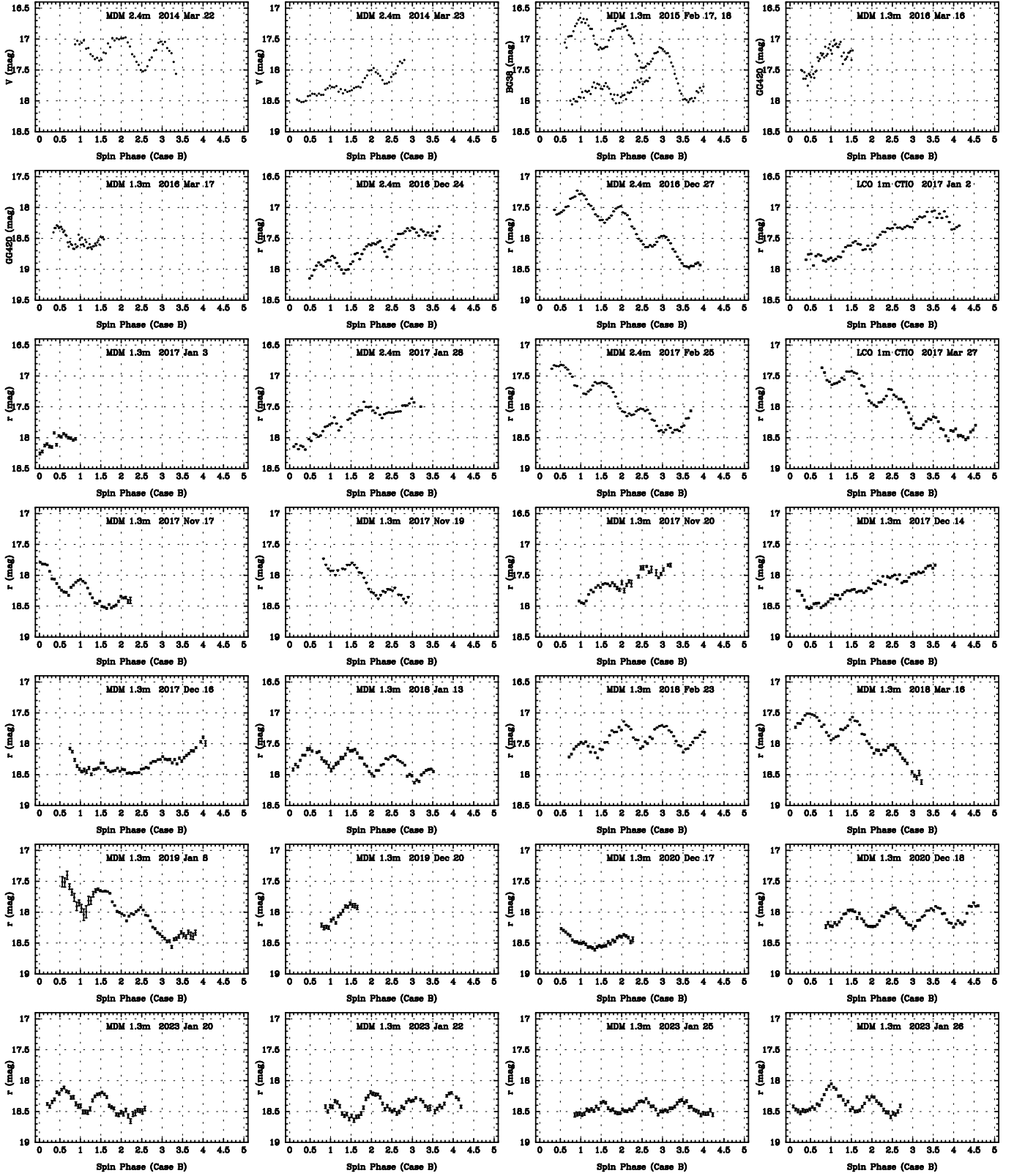


Figure 3. MDM and LCOGT light curves from 2014–2023, folded on the Case B spin period from Table 2. The six earliest light curves (from Paper 1), which were obtained with cadences of 5–20 s in a V , BG38, or GG420 filter, have been binned to either 150 s or 200 s to better match the signal-to-noise and 5 minute cadence of the subsequent r -band data.

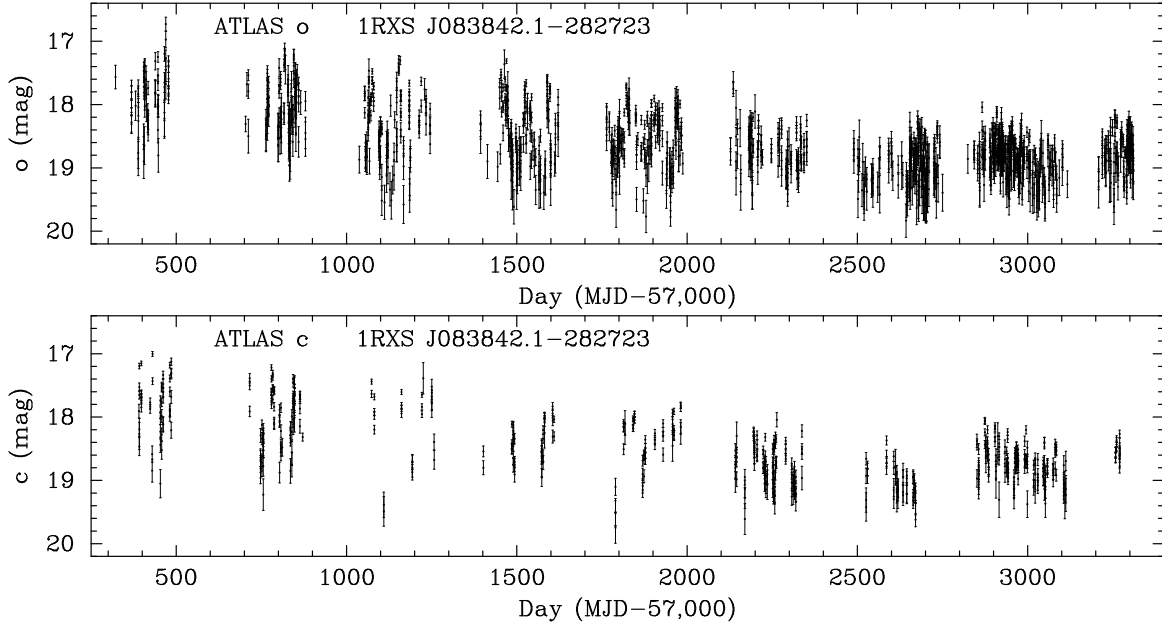


Figure 4. ATLAS photometry from 2015 October – 2023 December in the o and c filters.

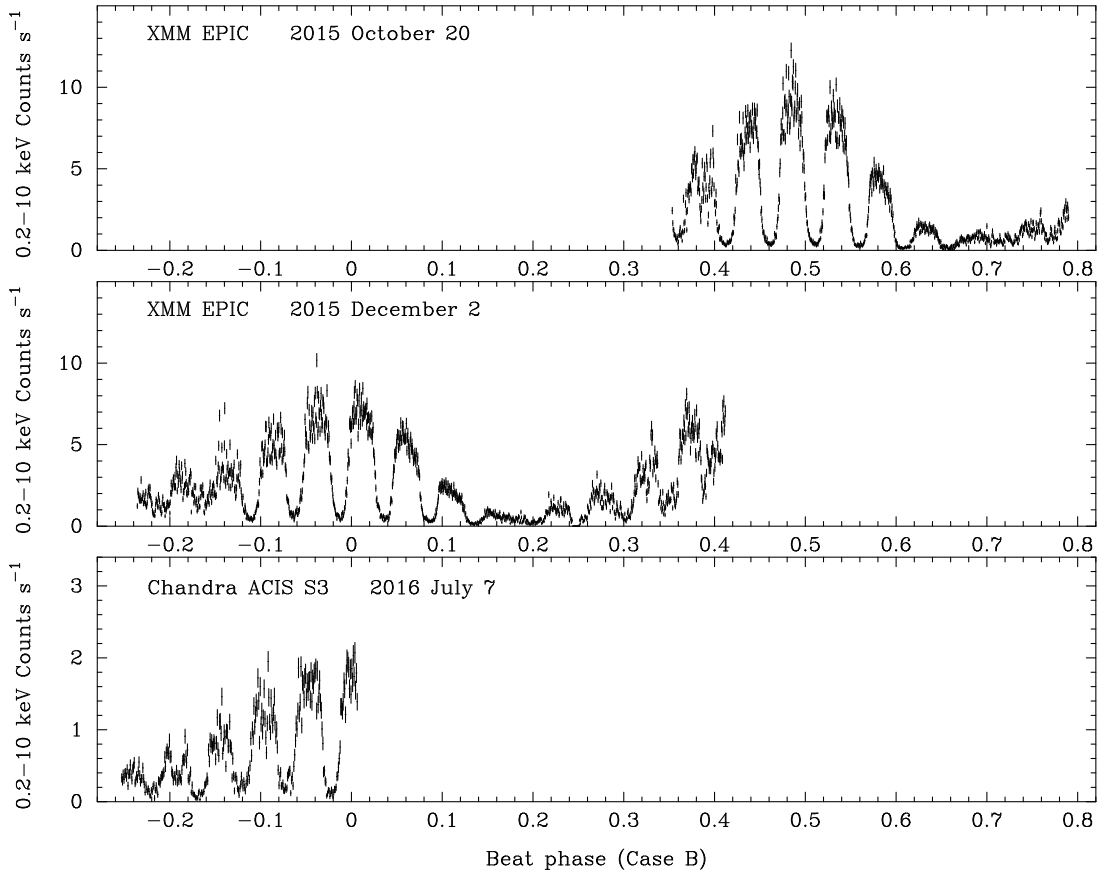


Figure 5. All X-ray light curves of RX J0838.7–2827 as a function of the Case B beat phase defined in Table 3.

Table 2. MDM/LCOGT Observed and Inferred Frequencies

Frequency (day ⁻¹)	Period	Case A	Case B
Observed			
1.489498(12)	16.11281(13) hr	$\omega_A - \Omega$	$2(\omega_B - \Omega)$
14.63083(5)	98.42230(37) min	Ω	Ω
16.12028(8)	89.32847(44) min	ω_A	$2\omega_B - \Omega$
Inferred			
0.744749(6)	32.22562(26) hr	...	$\omega_B - \Omega$
15.37556(10)	93.6552(6) min	...	ω_B

shown in Figure 4, where a slow decline of the mean magnitude from ≈ 17.8 to ≈ 19.0 is seen in both filters. Power-spectrum analysis of the barycentered data does not detect any significant periods, probably due to the sparse sampling. Nevertheless, it is evident that the day-to-day scatter in the points has become smaller in recent years, likely the effect of the decrease in the beat modulation seen in the TESS and most recent MDM data.

2.5. Constructing the Long-term Ephemerides

Only by combining the X-ray, TESS, and ground-based timing can precise beat, orbit, and pulse ephemerides be constructed that span 2014–2023. The X-ray observations were too far apart to count cycles between them and obtain more precise periods. Similarly, the TESS observation, even with its more precise periods, was too far removed from the X-ray observations to perform that phase linkage. However, once the TESS periods were used to identify the more precise corresponding values in the ground-based photometry, absolute phasing of all of the data follows.

All that remains is to define epochs of phase zero T_0 for each of the periods. For the orbital period, we use the epoch of blue-to-red crossing of the optical emission lines from Paper 1. For the spin period, we use the time of a *minimum* in the XMM-Newton light curve of Figure 1. Empirically, this is the most precise and least ambiguous fiducial, representing the center of the self-eclipse of an emitting pole by the WD. For the beat period, we estimate the time of *maximum* of the same X-ray light curve. The ephemerides so defined are given in Table 3.

The phases of the folded light curves in Figures 1–8 are all defined by these ephemerides. They reveal several model-independent relationships:

Table 3. Ephemeris Parameters

Quantity	T_0 (BJD)	Frequency ^a (day ⁻¹)
Orbit	2457408.8373(6) ^b	14.63083(5)
Case A		
Spin	2457359.741(1) ^c	16.12028(8)
Beat	2457359.76(1) ^d	1.489498(12)
Case B		
Spin	2457359.741(1) ^c	15.37556(10)
Beat	2457359.76(1) ^d	0.744749(6)

^aGround-based frequencies listed in Table 2.

^bEpoch of blue-to-red crossing of radial velocities from Paper 1, corrected to TDB.

^cMinimum of X-ray spin pulse profile in Figure 1.

^dMaximum of X-ray beat profile in Figure 1.

1. The optical beat is in phase with the X-ray beat (Figures 2, 5).
2. The X-ray observations together sampled all of the beat phases, even in Case B (Figure 5).
3. The optical spin profile is in phase with the X-ray spin profile (Figures 1, 3).
4. With phase 0 as the epoch of blue-to-red crossing, the optical continuum brightness is in phase with the radial velocity curve of the optical emission lines (Figures 1, 2, 6).

The implications of these results will be discussed in Section 3.

2.6. Phasing of Emission-Line Radial Velocities (2016)

Using the precise ephemerides of Table 3, we graph the 59 emission-line radial velocities from Paper 1, obtained in 2016 January–February, as a function of beat, orbit, and spin phase in Figure 6. As expected, there is no dependence on beat phase. The sinusoidal modulation that was attributed to the orbital period in Paper 1 is reproduced. But now we also fold at the candidate spin periods. In Case B this requires separating the points into two groups from different beat phases in order to search for effects of pole switching, as the TESS data were treated in Section 2.2.

In fact, modulation at the Case B spin period is almost as clear as it is on the orbital period, once the two halves of the beat cycle are separated, revealing spin cycles

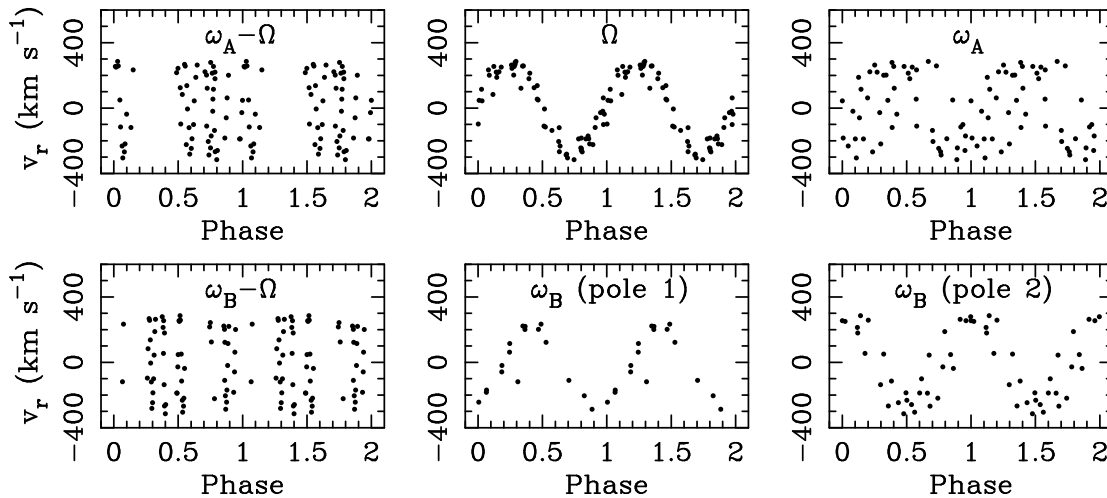


Figure 6. Radial velocities of $H\alpha$ emission from Paper 1, folded on the beat, orbital, and spin ephemerides of Table 3. Modulation is cleanest at the orbital period, but also strong at the Case B spin period when taking into account pole switching.

$\approx 180^\circ$ out of phase. Folding at the Case A spin period also shows significant modulation, but here the scatter is greater than in the Case B curves. The scatter is similar in magnitude to the drift in the X-ray and optical continuum pulses relative to the Case A spin ephemeris, which is discussed in Section 3.3. Figure 6 therefore suggests some preference for Case B over Case A.

Paper 1 concluded that the line-emitting region is fixed in the orbital frame, probably in the ballistic accretion stream. Now it seems equally possible that the line emission is coming from high in the magnetically confined accretion column, but fixed in the spinning frame. For pole 1, the maximum $H\alpha$ blueshift occurs at phase 0, when pole 1 is eclipsed, while for pole 2 the eclipse comes half a spin period later. Therefore, the velocities are all consistent with radial infall. The orbital longitude of the companion is not determined by the emission-line radial velocity curve, but it is likely that maximum blueshift at phase ≈ 0.75 in the Ω panel of Figure 6 corresponds to superior conjunction, with the accretion flow being nearly radial. With the reference frame of the emission lines being ambiguous, it is possible that both orbit and spin contribute.

3. DISCUSSION

3.1. Orbital Period

The goal of this study is to determine the true spin, orbit, and beat periods of RX J0838.7–2827, none of which was securely known. Our identification of the orbital period is supported by consistency between the emission-line radial velocity period and an identical optical photometric period. However, it is not obvious in the case of an AP whether the optical emission lines *should* be tied to the orbital frame of the secondary or the spinning frame of the WD. It would be logical to as-

sume the latter, that the strong magnetic field captures the ballistic stream high up and confines the emission-line region to the spinning frame.

Nevertheless, it is sometimes concluded that the emission-line radial velocity period is orbital when a different period in X-rays is judged more likely to be the spin, e.g., in IGR J19552+0043 (Tovmassian et al. 2017) and Swift J0503.7–2819 (Halpern 2022). In CD Ind and SDSS J134441.8+204408, Littlefield et al. (2019, 2023b) argued for a reinterpretation of the optical photometric period structure in TESS data that would allow the spectroscopic period, previously assumed to be orbital, to be the spin period. RX J0838.7–2827 presents a different problem in that pole switching in the radial velocities makes them identifiable to some extent with either frame, at least within the limited sampling of the existing spectroscopy. Tentatively, both orbit and spin frames could be represented in the emission lines. If photospheric absorption lines can be detected from the companion, perhaps in the new low state of accretion, at least its orbital period and epoch of ascending node could be securely determined.

The radial-velocity amplitude of $H\alpha$ emission in RX J0838.7–2827 is $274 \pm 16 \text{ km s}^{-1}$ (Paper 1), larger than that of most IPs, but similar to that of polars. Rea et al. (2017) decomposed higher-resolution emission-line profiles into three components, one with an even larger $\approx 1200 \text{ km s}^{-1}$ velocity amplitude that they attributed to the ballistic accretion stream. Both studies found that the equivalent width of the Balmer lines is higher (by a factor of $\lesssim 2$) when their radial velocity is maximally blueshifted. In Paper 1, we interpreted this to mean that the ballistic accretion stream is maximally blueshifted when the secondary is at superior conjunction, at the same time that the optical

continuum, produced lower in the accretion stream, is maximally occulted. TESS confirms that the optical continuum folded on our orbital frequency Ω is faintest at phase 0.75 (Figure 1), when the emission-line radial velocity is maximally blueshifted (Figure 6).

3.2. Beat Period

The beat period measured optically allows the X-ray light curves to be aligned in absolute beat phase in Figure 5, which we illustrate in Case B for evaluation of the ambiguity with Case A. If Case B applies, then both halves of the beat cycle were sampled by the combined XMM-Newton observations taken 43 days apart. But it is not clear from these light curves that the second half of the cycle, peaking at phase 0.5, differs in any way from the first half, peaking at phase 0. The similarity tends to argue instead for Case A.

The spin pulses have basically the same shape in X-rays during all parts of the beat cycle, with modulation of $\approx 100\%$. Their absolute flux changed modestly between the two XMM-Newton observations, but this may represent long-term variability of the accretion rate rather than a difference in the projected appearance of one pole versus the other. The longest light curve, from 2015 December 2, did not cover enough of the second half of the beat cycle to prove that the second half differs from the first half in detail. Thus, the evidence from X-rays alone does not strongly support Case B. At best, it requires a highly inclined and symmetric magnetic geometry to account for the strong spin modulation and similar pulse profile from both poles in Case B, perhaps with both poles in the same (upper) hemisphere. In addition, the accretion rate onto the WD has to go to zero during the switch between the poles, with matter perhaps stored in the accretion ring while the accretion stream is disconnected from either magnetic funnel.

In Case A, the beat modulation is caused by accretion switching from an upper pole to a lower pole that is mostly invisible; thus, the X-ray flux can go to zero at minimum without the total accretion rate having to modulate. It is an effect of small magnetic and observer inclination angles in Case A. However, the spin period required in Case A faces other issues, which will be discussed in the next Section.

The optical observations are possibly more definitive of the beat period due to their long duration covering many beat cycles. Analysis of the TESS data did isolate optical emission at the Case B spin period from two poles that differ in flux by $\approx 10\%$ averaged over the 50 days, and are aligned in phase with the X-ray pulses (Figure 1). This optical flux difference, also manifest as the fundamental and multiples of the Case B beat fre-

quency in the TESS power spectrum, appear to require Case B. The two unequal peaks in the ground-based beat profile (Figure 2) also favor Case B.

The multiple peaks in the TESS beat profile also suggests that the accretion rate was modulated in a more complex fashion in 2023, when the optical emission was low, than it was in the XMM-Newton observations of 2015 (which included the Optical Monitor) and the early ground-based observations, when the optical emission was brighter. It would now be most interesting to obtain a long X-ray observation in a low optical state. Since the potential locations of X-ray emission are more limited than the optical ones, the change in the accretion structure may be easier to diagnose in the X-ray.

3.3. Spin Period

The fast X-ray modulation is most naturally attributed to the spin period via self-occultation by the rotating WD of a shocked emitting region at the base of the accretion column. The observed dips are too broad to be due to eclipse by the orbiting secondary, or by the accretion stream. The value of the spin period follows directly from the beat period, or vice versa, because a single accreting pole is always dominant in the light curve in Case A, while two visible poles alternate during a twice longer beat period in Case B.

The period that most closely follows the X-ray and optical dips and peaks is the one that we infer is the spin period in Case B. This can be seen most easily in Figure 3 for the optical and Figure 7 for the X-ray. But this works only if there is complete pole switching, such that the spin phase jumps by half a spin cycle at the transition between each half of the beat cycle.

In contrast, neither the assumed orbital period nor the Case A spin period coincides with the phasing of the optical or X-ray modulation. This is seen in Figure 8, which tests the Case A spin period against the X-rays. Here the peaks drift by as much as $\pm 90^\circ$ in phase during each beat cycle. The same effect occurs in the ground-based optical data (the Case A version of Figure 3, not shown).

However, there is one caveat to this argument that may lend some support to Case A. As first argued by Geckeler & Staubert (1997), the footpoint of the accretion column on an AP is not expected to remain fixed on the surface of a WD. As the secondary transits over a magnetic pole, the accreting matter is captured and threaded onto successively different field lines. Looking from a fixed point on the WD, the secondary orbits in the retrograde direction if $\omega > \Omega$ as we infer here. The effect on the pulse timing is to shift it to earlier times at the beginning of the beat cycle, and to later times

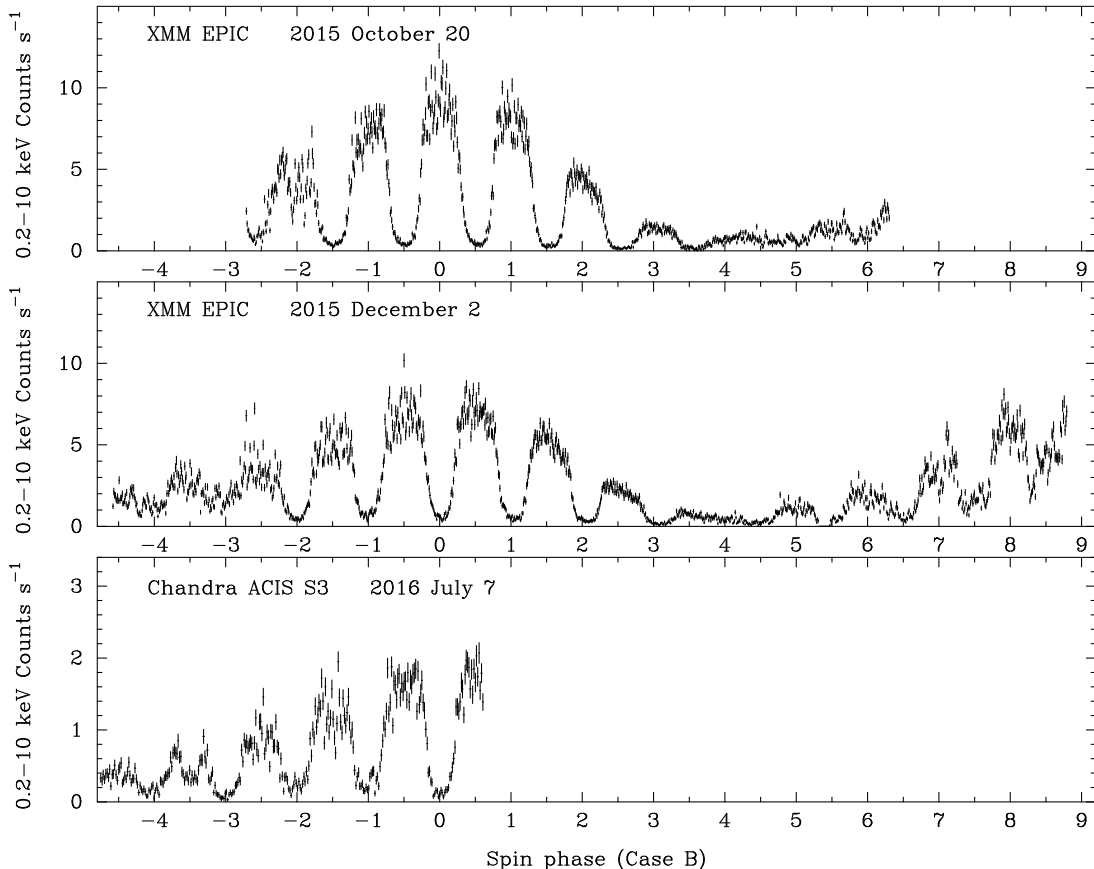


Figure 7. All X-ray light curves of RX J0838.7–2827 as a function of the Case B spin phase defined in Table 3.

at the end of the cycle, with respect to the mean spin ephemeris.

This is in fact the sense in which the phase drifts in the Case A interpretation (Figure 8) of RX J0838.7–2827. Such a spin-phase drift is also seen in other APs (Littlefield et al. 2019, 2023a), although it is not clear if the model of Geckeler & Staubert (1997) quantitatively explains the results. The shifts are predicted to be of order $\pm 20^\circ$ in longitude. For RX J0838.7–2827 in Case A, the drift of $\pm 90^\circ$ would imply that the accretion column travels half the circumference of the WD. That is, the footpoint of accretion approximately tracks the longitude of the companion. This would be an interesting challenge for modeling to address.

4. CONCLUSIONS

RX J0838.7–2827 has perhaps the simplest X-ray light curve of all APs, suggesting that the identification of its spin, orbital, and beat periods should be straightforward. We used TESS and ground-based optical timing to construct precise ephemerides for all of these periods, phased to the X-rays, as explained in the footnotes to Table 3. The original factor of 2 ambiguity in the beat period from the X-ray light curves appears to be resolved in favor of the longer beat period (Case B) by structure

in the optical beat profile, and complete pole switching between each half of the beat cycle as seen in the spin profile. It requires the spin frequency ω_B to be absent in the power spectrum, replaced by Ω and $2\omega_B - \Omega$. In this case $P_{\text{beat}} = 32.2256$ hr, $P_{\text{orb}} = 98.4223$ min, and $P_{\text{spin}}/P_{\text{orb}} = 0.95156$.

This conclusion is not obvious from the original X-ray observations. While it is possible that a longer X-ray observation would have revealed differences between adjacent halves of the beat cycle, they may be subtle, e.g., requiring there to be opposite poles at similar latitude in one equatorial hemisphere of the WD.

There is one important difference between the cases that is obvious in both X-ray and optical. Case B allows the footpoints of the accretion columns to remain relatively fixed on the surface of the WD, being phased well to the spin period. But if Case A is correct, the spin period is present in the power spectrum, and being shorter than in Case B, the footpoint of the single visible pole drifts in longitude almost halfway around the WD during each beat cycle. The plausibility of either of these dynamics should be tested by physical modeling.

An added complication is the long-term decline by ≈ 1 mag over the 9-year monitoring period, with its possible affect on the accretion rate and geometry. The

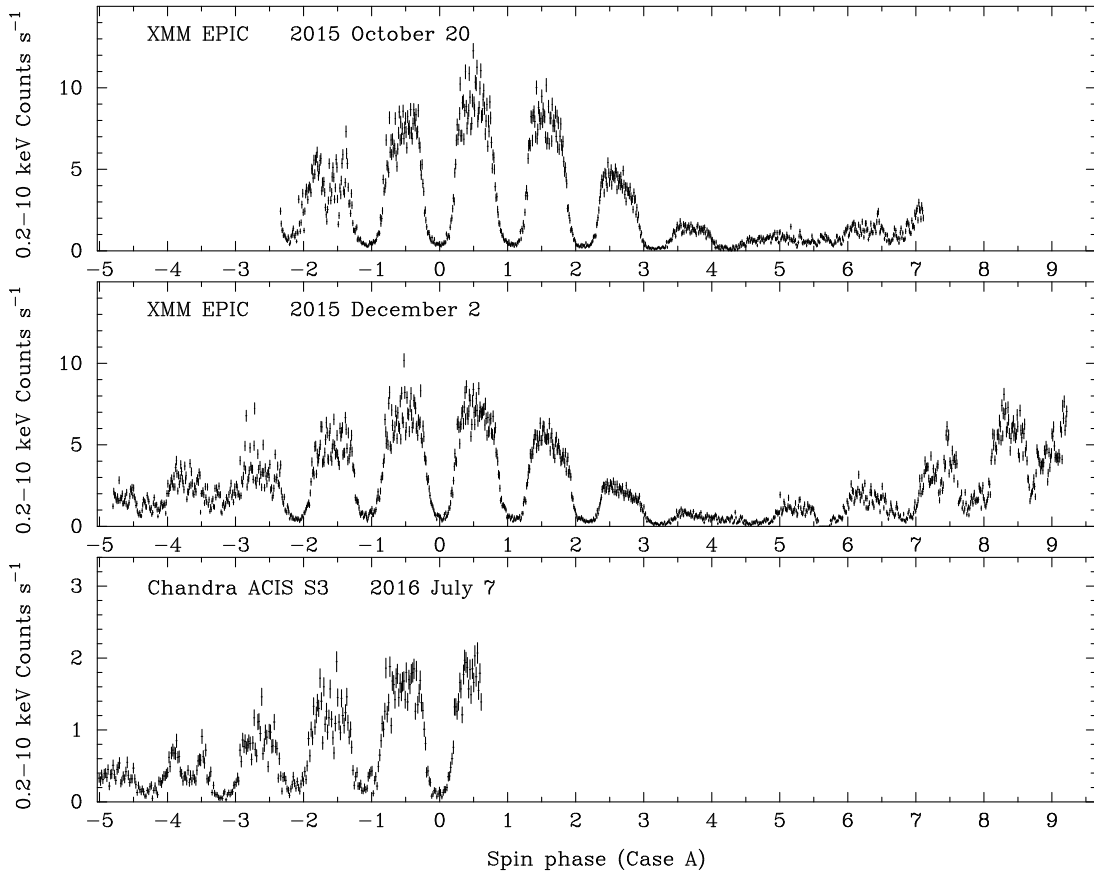


Figure 8. All X-ray light curves of RX J0838.7–2827 as a function of the Case A spin phase defined in Table 3.

X-ray and optical light curves obtained at the beginning of this period have simpler beat structure than the recent TESS observation made near minimum light. This could indicate a major change in the accretion flow, for which there is no contemporaneous X-ray comparison.

During previous XMM-Newton observations of RX J0838.7–2827 the Optical Monitor was not configured to resolve the orbit and spin modulations. A new, simultaneous X-ray/optical observation by XMM-Newton with its Optical Monitor in fast mode could reveal much about the accretion structure, including any state change. If spanning at least 32 hours, such an observation may, finally, decide the true spin and beat periods.

We thank the referee for a thorough evaluation of the manuscript. XMM-Newton is ESA science mission with instruments and contributions directly funded by ESA Member States and NASA. MDM Observatory is operated by Dartmouth College, Columbia University, The Ohio State University, Ohio University, and the University of Michigan. A Sinistro imager on a CTIO 1m telescope of the LCOGT network was also used. Data collected by the TESS mission were obtained from the MAST data archive at the Space Telescope Science Institute (STScI). The ATLAS science products were made possible through the contributions of the University of Hawaii Institute for Astronomy, the Queen’s University Belfast, the Space Telescope Science Institute, the South African Astronomical Observatory, and The Millennium Institute of Astrophysics (MAS), Chile.

Facility: XMM, McGraw-Hill, Hiltner, LCOGT, TESS.

REFERENCES

- Gaia Collaboration, Prusti, T., de Bruijne, J. H. J., et al. 2016, *A&A*, 595, A1, doi: [10.1051/0004-6361/201629272](https://doi.org/10.1051/0004-6361/201629272)
- Gaia Collaboration, Bailer-Jones, C. A. L., Teyssier, D., et al. 2023, *A&A*, 674, A41, doi: [10.1051/0004-6361/202243232](https://doi.org/10.1051/0004-6361/202243232)

- Geckeler, R. D., & Staubert, R. 1997, *A&A*, 325, 1070
- Halpern, J. P. 2022, *ApJ*, 934, 123,
doi: [10.3847/1538-4357/ac7d50](https://doi.org/10.3847/1538-4357/ac7d50)
- Halpern, J. P., Bogdanov, S., & Thorstensen, J. R. 2017,
ApJ, 838, 124, (Paper 1),
doi: [10.3847/1538-4357/838/2/124](https://doi.org/10.3847/1538-4357/838/2/124)
- Joshi, A., Pandey, J. C., Singh, K. P., & Agrawal, P. C.
2016, *ApJ*, 830, 56, doi: [10.3847/0004-637X/830/2/56](https://doi.org/10.3847/0004-637X/830/2/56)
- Kolbin, A. I., Suslikov, M. V., Kochkina, V. Y., et al. 2024,
Astronomy Letters, 49, 475,
doi: [10.1134/S1063773723080029](https://doi.org/10.1134/S1063773723080029)
- Littlefield, C., Garnavich, P., Mukai, K., et al. 2019, *ApJ*,
881, 141, doi: [10.3847/1538-4357/ab2a17](https://doi.org/10.3847/1538-4357/ab2a17)
- Littlefield, C., Hoard, D. W., Garnavich, P., et al. 2023a,
AJ, 165, 43, doi: [10.3847/1538-3881/aca1a5](https://doi.org/10.3847/1538-3881/aca1a5)
- Littlefield, C., Mason, P. A., Garnavich, P., et al. 2023b,
ApJL, 943, L24, doi: [10.3847/2041-8213/acaf04](https://doi.org/10.3847/2041-8213/acaf04)
- Myers, G., Patterson, J., de Miguel, E., et al. 2017, *PASP*,
129, 044204, doi: [10.1088/1538-3873/aa54a8](https://doi.org/10.1088/1538-3873/aa54a8)
- Norton, A. J., Butters, O. W., Parker, T. L., & Wynn,
G. A. 2008, *ApJ*, 672, 524, doi: [10.1086/523932](https://doi.org/10.1086/523932)
- Norton, A. J., Wynn, G. A., & Somerscales, R. V. 2004,
ApJ, 614, 349, doi: [10.1086/423333](https://doi.org/10.1086/423333)
- Pradeep, K. G., Singh, K. P., Dewangan, G. C., et al. 2024,
MNRAS, 527, 774, doi: [10.1093/mnras/stad3139](https://doi.org/10.1093/mnras/stad3139)
- Rawat, N., Pandey, J. C., Joshi, A., Scaringi, S., & Yadava,
U. 2022, *MNRAS*, 517, 1667,
doi: [10.1093/mnras/stac2723](https://doi.org/10.1093/mnras/stac2723)
- Rea, N., Coti Zelati, F., Esposito, P., et al. 2017, *MNRAS*,
471, 2902, doi: [10.1093/mnras/stx1560](https://doi.org/10.1093/mnras/stx1560)
- Ricker, G. R., Winn, J. N., Vanderspek, R., et al. 2015,
*Journal of Astronomical Telescopes, Instruments, and
Systems*, 1, 014003, doi: [10.1117/1.JATIS.1.1.014003](https://doi.org/10.1117/1.JATIS.1.1.014003)
- Schwarz, R., Schwöpe, A. D., Staude, A., et al. 2007, *A&A*,
473, 511, doi: [10.1051/0004-6361:20077684](https://doi.org/10.1051/0004-6361:20077684)
- Tonry, J. L., Denneau, L., Heinze, A. N., et al. 2018, *PASP*,
130, 064505, doi: [10.1088/1538-3873/aabadf](https://doi.org/10.1088/1538-3873/aabadf)
- Tovmassian, G., González-Buitrago, D., Thorstensen, J.,
et al. 2017, *A&A*, 608, A36,
doi: [10.1051/0004-6361/201731323](https://doi.org/10.1051/0004-6361/201731323)
- Wang, Q., Qian, S., Han, Z., et al. 2020, *ApJ*, 892, 38,
doi: [10.3847/1538-4357/ab7759](https://doi.org/10.3847/1538-4357/ab7759)